Ab initio calculation of x-ray absorption of iron up to 3 Mbar and 8000 K

Stéphane Mazevet, Vanina Recoules, Johan Bouchet, François Guyot, M. Harmand, Alessandra Ravasio, Alessandra Benuzzi-Mounaix

PHYSICAL REVIEW B **89**, 100103(R) (2014)

Ab initio calculation of x-ray absorption of iron up to 3 Mbar and 8000 K

S. Mazevet,[1,2,*] V. Recoules,[1,2] J. Bouchet,[1,2] F. Guyot,[3] M. Harmand,[4] A. Ravasio,[1,4] and A. Benuzzi-Mounaix[1,4]

[1]*LUTH UMR8102, Observatoire de Paris, CNRS, Université Paris Diderot, F-92195 Meudon, France*

[2]*CEA-DAM-DIF, F-91297 Arpajon, France*

[3]*IMPMC, MNHN, UPMC, UMR CNRS 75-90, Sorbonne Université, Paris, France*

[4]*LULI, Ecole Polytechnique, CNRS, CEA, UPMC, route de Saclay, F-91128 Palaiseau, France*

(Received 22 March 2013; revised manuscript received 28 January 2014; published 13 March 2014)

Using *ab initio* simulations within the generalized gradient approximation, we calculate x-ray absorption near edge spectra (XANES) at the iron *K* edge throughout the high-pressure phase diagram and up to extreme density and temperature conditions that are representative of the Earth's inner core (up to 3 Mbar and 8000 K). We show that XANES spectra near the Fe *K* edge exhibit clear signatures for the different high-temperature, high-pressure phases of iron. This suggests that XANES spectroscopy might be used to resolve ongoing controversies regarding both the high-pressure melting curve of iron and the nature of the solid phases undergoing melting up to several Mbar. In contrast to diffraction measurements, it also offers a severe constraint for density functional theory predictions of the transport properties of iron by providing direct information on the electronic structure of iron at these extreme conditions.

DOI: 10.1103/PhysRevB.89.100103 PACS number(s): 71.22.+i, 51.30.+i, 51.70.+f, 52.50.Jm

Understanding the behavior of matter under extreme density-temperature conditions is a key issue for various fields of physics ranging from designing new materials, enabling inertial confinement fusion using high power lasers, or modeling planets both within and outside our solar system [1]. Among a few key elements, the high-temperature, high-pressure phase diagram of iron, the main component of the Earth's core, has attracted a lot of attention in the past five decades. Despite this intense activity, several issues, such as the magnetic and transport properties at high pressures, the crystal structure at the Earth's inner core, and the corresponding melting temperature, still remain the subject of intense debates [2].

On the theoretical side, various density functional theory (DFT) approximations have been used to establish the high-pressure phase diagram for iron. They extend from lattice dynamics calculations that neglect the effect of anaharmonicity and are only valid at low temperatures [3] (i.e., below a few thousand degrees Kelvin), to full molecular dynamics simulations [4,5] based on finite temperature DFT. The latter gives access to the high-pressure melting curve and to the high-temperature, high-pressure phase diagram [6]. Combined with linear response theory as expressed within the Kubo-Greenwood formulation, this method also provides a complete set of transport properties consistent with the obtained equation of state [7,8]. These studies are so far mostly based on the local density approximation (LDA) or generalized gradient approximation (GGA) and leave open the issue of correlation at extreme conditions and of its potential impact on the magnetic and transport properties [9].

On the experimental side, static experiments combined with x-ray diffraction measurements have established the high-pressure melting curve up to 2 Mbar but with a location of the (γ,ϵ,liq) triple point that varies between 0.6 and 1.3 Mbar [10]. Above 2 Mbar, shock techniques are formally the most promising approach. Recently, a first step toward a consensus between static and dynamical experiments [10] has been reached by using diffraction measurements on static compression experiments. However, uncertainties between the two approaches will remain as long as the solid-liquid transition is not directly observed using a structural diagnostics during dynamic compression. Furthermore, measurements concerning transport properties such as thermal conductivity or magnetic properties at extreme conditions that are needed for planetary modeling are mostly nonexistent. Current estimates for these properties based on DFT predictions require experimental validations that could be provided by direct information on the changes taking place at the electronic structure level. X-ray absorption near edge spectra (XANES) measurements that are routinely performed in static experiments could provide such a constraint [11]. It was also recently developed in dynamical experiments using high power lasers to study phase transitions during isochoric heating by a proton beam [12], along the aluminum shock Hugoniot [13], and to study the nonmetal-metal transition during the release of an aluminum plasma [14].

We show here that clear signatures exist in the iron XANES spectra that identify solid-solid as well as solid-liquid phase transitions. The agreement obtained between our calculated spectra and experimental data at low pressures suggests that XANES measurements near the *K* edge of iron that can be performed in both static and dynamical experiments could help resolve the longstanding controversy regarding the high-pressure melting temperature of iron above 1 Mbar. In addition to diffraction measurements that only provide information on the underlying crystallographic phase, XANES measurements also provide some information on the electronic structure at these extreme conditions. This could potentially bring additional constraints for DFT calculations at these conditions and increase confidence in the transport properties calculated for planetary modeling where no experimental data are available.

To demonstrate the reliability of the XANES diagnostic to identify the crystallographic phases, we calculate XANES spectra using *ab initio* calculations across the α-ϵ phase transition around 15 GPa where experimental data are available, at varying temperatures along the normal density isochore (ρ = 7.85 g/cm^3) and around the high-pressure melting curve [5].

*stephane.mazevet@obspm.fr

For the latter, we investigated one condition well accessible to static measurements at about 60 GPa, one close to the shock Hugoniot at around 160 GPa, and one at Earth's core conditions at about 330 GPa. This is potentially accessible using quasi-isentropic compression schemes [15,16].

To simulate these thermodynamic conditions, we performed molecular dynamics simulations using typically 128 atoms in the simulation cell as described in detail in Ref. [5]. We used projected augmented wave (PAW) pseudopotentials generated using the ATOMPAW package [17] with $3s$, $3p$, $3d$, and $4s$ states as valence electrons. The cutoff radius was set at $2.1a_B$ to access the highest density investigated here. The electronic structure calculations were performed using the generalized gradient approximation (GGA) according to the parametrization of Perdew, Burke, and Ernzerhof (PBE) for the exchange-correlation energy and potential [18]. Details on the PAW pseudopotential generation as well as a comparison of the calculated 300 K isotherm with experimental data can be found in Ref. [19].

The *ab initio* molecular dynamics (AIMD) simulations were performed using a cutoff energy for the plane wave basis chosen as equal to 350 eV. We performed simulations using the ABINIT code [20]. We used the isokinetics ensemble where the number of particles, volume, as well as temperature are held fixed during the simulation. In this ensemble, the temperature is kept constant by rescaling the velocities at each time step. All the simulations were performed at the Γ point where the required convergence in both internal energy and pressure were achieved. For the conditions along the high-pressure melting curve, we directly simulated the solid and liquid phases following the results given in Ref. [5]. For the normal density isochore, we simulated the phases given by the experimental phase diagram.

For a given trajectory, we chose several snapshots to calculate the optical response in the x-ray domain using the linear response theory as expressed within the Kubo-Greenwood formulation [21]. For the optical properties, we used a $2 \times 2 \times 2$ **k**-point grid as defined within the Monkhorst-Pack scheme [22]. In contrast to previous calculations performed on Al [21], we did not use the impurity model to calculate the x-ray absorption cross section. In this framework, an "excited" pseudopotential is used for the excited atom in the calculation of the cross section to account for the particle-hole interaction. As already noted for other metals [23], in the case of iron, we did not find significant differences in the resulting cross sections using this model. We thus chose to describe the absorbing atom using the same pseudopotential as used in the molecular dynamics simulations. In this situation, we calculated the x-ray absorption cross section for all the atoms in the simulation cell for each snapshot and averaged over both atoms and snapshots.

Figure 1 shows the XANES spectrum obtained at normal density ($\rho_0 = 7.84$ g/cm^3) using a Gaussian broadening of 2.7 eV in the calculations. At zero temperature, where the atoms are in perfect body-centered-cubic (bcc) positions, the XANES spectrum (green curve) exhibits distinct structures above the edge. They are denoted as (a,b,c,d) in Fig. 1. At 300 K (black curve), the XANES spectrum still shows the four structures pointed out at zero temperature but with a significant broadening. We note that the effect of temperature on the

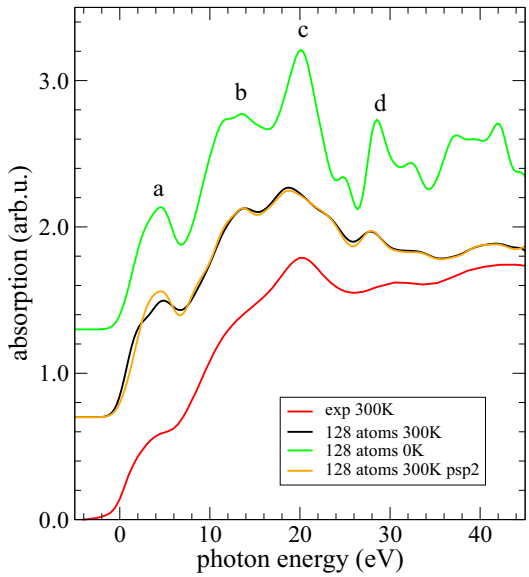

FIG. 1. (Color online) Comparison between the *ab initio* and experimental XANES spectra at normal conditions $\rho = \rho_0$. The spectra are shifted vertically for clarity. The positions in energy are normalized to the experimental value taken as the reference energy.

XANES spectrum results first from the thermal motion of the ions around their equilibrium positions. This is captured using various snapshots along the molecular dynamics trajectory. The effect of temperature also arises from the use of finite temperature DFT where the Kohn-Sham orbitals are populated according to a Fermi-Dirac distribution. At 300 K, our calculations show that the electronic temperature only leads to a slight broadening of the edge that remains barely noticeable. At this temperature, the broadening mainly arises from the thermal motion of the ions.

When comparing to the experimental spectrum [24] (red curve), we find a rather good agreement. We recover the four structures noted above (a,b,c,d) even if they are slightly more pronounced in the calculations. The largest discrepancy is noticeable at the highest photon energies and beyond the structure denoted as (d). In this region, we obtain a different slope between the calculated and measured spectra. The calculated x-ray absorption decreases at the highest energies while the measured one shows a slightly positive increase as a function of photon energy. To check whether the agreement could be improved, we designed a PAW pseudopotential with an additional p projector at higher energy (orange curve) and also increased the size of the simulation cell to 250 atoms. Overall, we found that the calculation is rather insensitive and robust with respect to the size or the type of the local PAW basis. By increasing the size of the simulation cell, we observed differences at photon energies above the (d) structures. This indicates that the spectrum is well converged with respect to the particle number up to 30 eV above the edge. Beyond this photon energy, the differences between the two spectra suggest that an even larger number of particles may be required to improve the agreement with the experimental data. This is, however, beyond the scope of this study and out of reach using current computational facilities. We will thus concentrate on the first 30 eV above the edge in the rest of this study.

We further point out that the XANES cross section near the K edge remains mostly unchanged when calculated within the spin polarized approximation. This is, at first glance, surprising as it is well known that iron is ferromagnetic in the α phase. It is also critical to perform a spin polarized calculation in order to obtain the proper equation of state in the α phase and to bring the equilibrium volume in better agreement with the experiment. This little sensitivity to spin can be understood by considering that iron is a transition element with a partially filled d shell. The dominant contribution to the density of states near and above the Fermi level comes from the d band. The magnetic properties of iron mostly stem from the d band while the XANES cross section near the K edge is proportional to the partial p-DOS. The calculations indicate that the p-DOS appears rather insensitive to spin. Direct information on the magnetic properties would be accessible via the L-edge cross section that depends on the partial d-DOS. The energy of the edge is, however, too low to be of use in dynamical experiments with currently available sources. Having established the accuracy of the method at describing the XANES spectrum at normal conditions, we now turn to its evolution along the pressure induced α-ϵ phase transition occurring at around 15 GPa.

In Fig. 2, we compare the spectra obtained in the α (bcc) and ϵ (hcp) phases with the experimental measurements [24]. To highlight the sensitivity of the XANES spectrum to the underlying crystal structure, we performed, for each phase, calculations at pressures above and below the phase transition. We see in Fig. 2 that for a given phase, the XANES spectrum barely depends on pressure. On the other hand, clear differences are noticeable between the two phases throughout this pressure region. The structure denoted as (a) in the bcc spectrum is shifted to higher energies in the hcp spectrum while the (b) and (c) features are mostly disappearing for the first one and shifting to lower energies for the second. When comparing to the experimental spectra, we can now clearly identify that a bcc-hcp phase transition occurred in this pressure range by comparing with the *ab initio* calculations. Indeed, we see

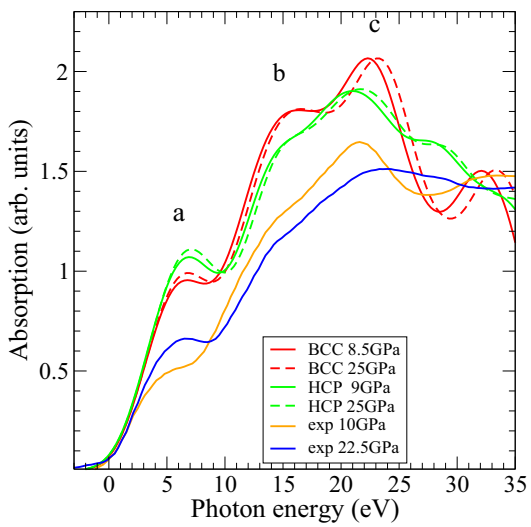

FIG. 2. (Color online) Comparison between the calculated and experimental spectra across the α-ϵ transition. Experimental data are from Ref. [24].

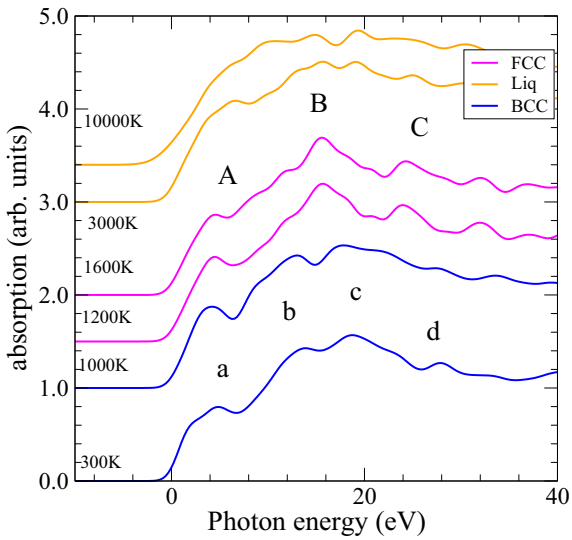

FIG. 3. (Color online) Variation of the XANES spectrum as a function of temperature at normal density $\rho = \rho_0$. The spectra are shifted for clarity and their positions in energy are normalized to the experimental value taken as the reference energy.

that the experimental spectrum coincides with the bcc one at 10 GPa and the hcp one at 22.5 GPa. Furthermore, it is worth pointing out that this identification is made by using the 30 eV photon energy range. Having established that the K-edge XANES spectrum carries information on the crystallographic phase that can be measured experimentally, we now turn to its evolution in temperature along the (α-γ) transition and along the high-pressure melting curve.

Figure 3 shows the variation of the XANES spectrum as temperature increases up to 10 000 K and as the system evolves from a magnetic bcc to a nonmagnetic face-centered-cubic (fcc) state and, finally, into a liquid. We see that the four structures identified above as (a,b,c,d) remain up to the solid-solid phase transition that occurs close to the Curie temperature ($T_C = 1100$ K). As the system turns into an fcc state, we see that the b and c structures disappear. They are replaced by a broader structure denoted as B in Fig. 3. The minimum in the fcc spectrum in between the structures identified as B and C occurs at energies corresponding to a maximum labeled c in the bcc spectrum. This significant change in the spectrum across the α-γ phase transition is consistent with the experimental measurements reported by Filipponi *et al.* [25]. As the temperature further increases and the system turns into a liquid, most structures disappear. The A and B structures significantly broaden upon melting and the spectrum becomes structureless at the highest temperature.

Figure 4 shows the variation of the XANES spectrum along the high-pressure melting curve of iron. We chose three isochores: one that can be reached using a laser heated diamond anvil cell (DAC) ($\rho = 10$ g/cm^3; $P = 60$ GPa), one along the principal shock Hugoniot ($\rho = 12$ g/cm^3; $P = 160$ GPa), and one at the Earth's core conditions ($\rho = 13.15$ g/cm^3; $P = 330$ GPa). At each condition, we calculated the XANES spectrum at temperatures above and below the melting temperature and applied only half the Gaussian broadening used at the previous conditions (1.3 eV). For the solid phases, we calculate

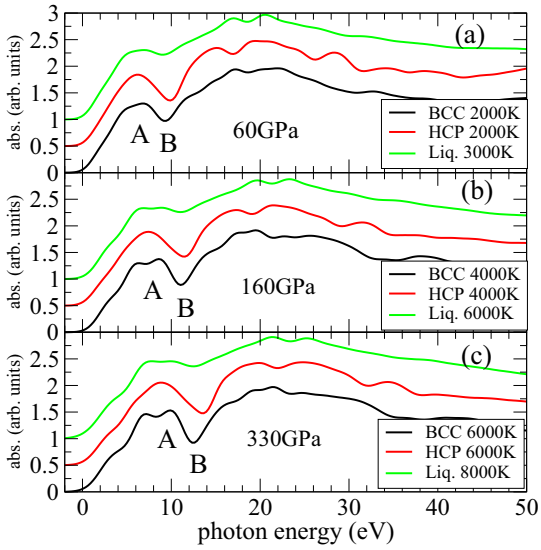

FIG. 4. (Color online) XANES spectra for the bcc, hcp, and liquid phases along the high-pressure melting curve. The spectra are shifted in energy for clarity and their positions in energy are normalized to the experimental value at normal conditions taken as the reference energy, disregarding the energy shift due to density.

the x-ray absorption for both the bcc and hcp phases as there is currently some uncertainty regarding the high-temperature solid phase for iron. While the bcc phase is dynamically unstable at 0 K, *ab initio* simulations indicate that it becomes stable in temperature [5]. The difference in free energy between the two phases remains, however, within the error bars of the calculations. The verdict is thus still out regarding the high-pressure solid phase of iron close to melting [5].

We see in Fig. 4 that the XANES spectra show identifiable signatures for the different phases up to the highest pressure. At this lower resolution, the feature denoted as a in the previous figures is now identified as A and B. For the three conditions studied here, the XANES spectra calculated in the bcc phase show a double maximum near the edge, denoted as A in Fig. 4, followed by a sharp minimum (denoted as B). This minimum appears consistently at about 10 eV after the edge and up to a pressure of 3 Mbar. In the hcp phase, the double maximum denoted as A is replaced by a single maximum. This maximum is also followed by a sharp minimum as in the bcc phase. We note, however, that this minimum appears consistently at a photon energy that is higher by about 2 eV than in the bcc phase. At a given condition, this shows that the position of this minimum (feature B) and the shape of the first maximum (feature A) may allow one to discriminate between the two solid phases. From the experimental point of view, resolving the bcc and hcp iron phases based on these features would only require an experimental resolution of about 1 eV as well as a signal fluctuation of a few percent. As demonstrated above for the (α,ϵ) transition, these features will be bring sufficient differences in a lower resolution spectrum to enable one to discriminate between the two phases when compared to the *ab initio* simulations results.

A clear result shown in Fig. 4 is that XANES measurements could bring relevant information on the longstanding problem of high-pressure melting in iron. Indeed, Fig. 4 shows that the minimum previously denoted as B has mostly disappeared in the liquid state. We further point that this is not gradual but an abrupt change directly related to the underlying phase. It shows that an experimental resolution of about 1 eV should enable one to discriminate between the liquid and solid states using only this feature in the XANES spectrum up to conditions encountered in the Earth's core. We further point out that this could be achieved even if the solid phase cannot be clearly identified. Again, a direct comparison with the *ab initio* simulation results over the first 30 eV above the edge would probably enable this identification with a lower experimental resolution.

In summary, by exploring a broad range of density and temperature conditions using *ab initio* simulations, we showed that XANES measurements can be very useful to establish the high-pressure, high-temperature phase diagram of iron. We identified several signatures corresponding to the solid and liquid phases currently predicted up to the Earth's core conditions. While less direct than diffraction measurements as they require a comparison with first principles simulations, XANES measurements present the advantage of providing information on the electronic structure of iron at extreme conditions. This would potentially bring confidence in the transport properties calculated using the DFT approximation at extreme conditions.

[1] M. D. Knudson, M. P. Desjarlais, R. W. Lemke, T. R. Mattsson, M. French, N. Nettelmann, and R. Redmer, Phys. Rev. Lett. **108**, 091102 (2012); R. S. McWilliams, D. K. Spaulding, J. H. Eggert, P. M. Celliers, D. G. Hicks, R. F. Smith, G. W. Collins, and R. Jeanloz, Science **338**, 1330 (2012); R. Chau, S. Hamel, and W. J. Nellis, Nat. Commun. **2**, 203 (2011).

[2] S. Anzellini, A. Dewaele, M. Mezouar, P. Loubeyre, and G. Morard, Science **340**, 464 (2013); S. Tateno and K. Hirose, *ibid.* **330**, 359 (2010); R. Boehler, Nature (London) **363**, 534 (1993), and references therein.

[3] L. Stixrude, Phys. Rev. Lett. **108**, 055505 (2012).

[4] D. Alfe, Rev. Mineral. Geochem. **71**, 337 (2010).

[5] J. Bouchet, S. Mazevet, G. Morard, F. Guyot, and R. Musella, Phys. Rev. B **87**, 094102 (2013); L. Vocadlo *et al.*, Nature (London) **424**, 536 (2003).

[6] J. Bouchet, D. Valencia, S. Mazevet, and F. Guyot, High Energy Density Phys. **7**, 111 (2011).

[7] S. Mazevet, M. Torrent, V. Recoules, and F. Jollet, High Energy Density Phys. **6**, 84 (2010).

[8] M. Pozzo, C. Davies, D. Gubbins, and D. Alfe, Nature (London) **485**, 355 (2012).

[9] L. V. Pourovskii, T. Miyake, S. I. Simak, A. V. Ruban, L. Dubrovinsky, and I. A. Abrikosov, Phys. Rev. B **87**, 115130 (2013).

[10] A. Dewaele, M. Mezouar, N. Guignot, and P. Loubeyre, Phys. Rev. Lett. **104**, 255701 (2010).

[11] J. J. Rehr and R. C. Albers, Rev. Mod. Phys. **72**, 621 (2000).

[12] A. Mancic, A. Levy, M. Harmand *et al.*, Phys. Rev. Lett. **104**, 035002 (2010).

[13] A. Benuzzi-Mounaix, F. Dorchies, V. Recoules, F. Festa, O. Peyrusse, A. Levy, A. Ravasio, T. Hall, M. Koenig, N. Amadou, E. Brambrink, and S. Mazevet, Phys. Rev. Lett. **107**, 165006 (2011).

[14] A. Levy, F. Dorchies, A. Benuzzi-Mounaix *et al*., Phys. Rev. Lett. **108**, 055002 (2012).

[15] A. Benuzzi-Mounaix, S. Mazevet, A. Ravasio *et al*., Physica Scripta **T159** (2014) (to be published).

[16] R. Boehler, Musshoff HG, R. Ditz, G. Aquilanti, and A. Trapananti, Rev. Sci. Instrum. **80**, 045103 (2009).

[17] N. A. W. Holzwarth, A. R. Tackett, and G. E. Matthews, Comput. Phys. Commun. **135**, 329 (2001).

[18] J. P. Perdew, K. Burke, and M. Ernzerhof, Phys. Rev. Lett. **77**, 3865 (1996).

[19] A. Dewaele, M. Torrent, P. Loubeyre, and M. Mezouar, Phys. Rev. B **78**, 104102 (2008).

[20] X. Gonze *et al*., Comput. Mater. Sci. **25**, 478 (2002); Comput. Phys. Commun. **180**, 2582 (2009).

[21] S. Mazevet and G. Zerah, Phys. Rev. Lett. **101**, 155001 (2008); V. Recoules and S. Mazevet, Phys. Rev. B **80**, 064110 (2009).

[22] H. J. Monkhorst and J. D. Pack, Phys. Rev. B **13**, 5188 (1976).

[23] V. Mauchamp, M. Jaouen, and P. Schattschneider, Phys. Rev. B **79**, 235106 (2009).

[24] O. Mathon, F. Baudelet, J. P. Itie, A. Polian, M. d'Astuto, J.C. Chervin, and S. Pascarelli, Phys. Rev. Lett. **93**, 255503 (2004).

[25] A. Filipponi, M. Borowski, P. W. Loeffen, S. De Panfilis, A. Di Cicco, F. Sperandini, M. Minicucci, and M. A. Giorgetti, J. Phys: Condens. Matter **10**, 235 (1998).